A Model Simulation of the Summer Circulation from the Eastern Mediterranean past Lake Kinneret in the Jordan Valley

P. ALPERT,[1] A. COHEN AND J. NEUMANN

The Hebrew University, Jerusalem, Israel

E. DORON

Israel Atomic Energy Commission, Nuclear Research Centre, Negev, Israel

(Manuscript received 10 August 1981, in final form 30 April 1982)

ABSTRACT

A model is described for the representation and study of air flow from the eastern Mediterranean (on the west side of the model's domain) past Lake Kinneret in the Jordan Valley (about 210 m below MSL) and beyond to the east (on the east side of the model) in the summer months. The primary purpose of the model is to improve our understanding of two striking features of the meteorology of the lake area in summer: 1) the almost daily development of strong winds and an associated storm on the lake in the afternoon, and 2) a nearly 50% drop in wind speed across the lake, from the western to the eastern shore, over a distance of only 10 km, again in the afternoon.

The model is two-dimensional. It uses the sigma coordinate system and is thus hydrostatic. The horizontal grid distance is 4 km. It has 10 levels in the vertical, between the surface and the top at 750 mb. The first level in the vertical is 10 m above the surface and each of the higher levels is at an altitude that is approximately twice the altitude of the next *lower* level.

In the numerical scheme we apply Marchuk's splitting method: a numerical filter is applied in the horizontal which suppresses short waves but leaves the long waves relatively unaffected. The time step is 8 s.

The results indicate the development of strong winds on the west side of the lake in the afternoon. These winds are explained by the model as being the sudden incursion of the cool Mediterranean sea breeze front to the relatively warm Kinneret Valley. The strong intensity is explained by the dynamic effect of the hills with a contribution due to the collapse of an opposing upslope valley breeze. It is also suggested that an important contribution to the downslope acceleration is made by the onset of a density current when relatively cool Mediterranean air penetrates the warm air in the valley. The model needs further improvement since the time of onset of the strong winds is about 1.5 h late compared with observations. The weakening of the winds from the west shore to the east shore is well simulated by the model.

1. Introduction

One of the striking meteorological phenomena of the summer season in the Jordan Valley is the development of strong westerly winds, reaching 10–15 m s^{-1}, from the direction of the Mediterranean, during the afternoon. Another feature of interest is the suddenness with which the winds gain speed early in the afternoon. The diurnal variation of the surface wind in summer, representing two weeks of measurements (Serruya, 1975), is shown for two points along the lake shore in Fig. 1. One point is on the northwestern shore, the other on the southeastern side (see Fig. 2).

There is little doubt that these winds are a transformation of the Mediterranean sea breeze (MSB) which is an almost daily feature of the summer in Israel. Lake Kinneret (the Sea of Galilee), which is located in the northern section of the Jordan Valley, is ~45 km east of the Mediterranean coast. The MSB, in the form of a west wind, arrives in the lake area about 1300–1400 LST. As the winds move toward the lake, they "climb" hills 400 m high, and after crossing the hills descend eastward to the Jordan Valley, which is at 210 m below MSL. Thus, the winds descend from the hill tops a total of ~600 m. Also, while in the Mediterranean coastal plain, the MSB has a speed of 5–6 m s^{-1}, in the Jordan Valley the speed of the afternoon wind reaches, as was mentioned above, 10–15 m s^{-1}. These winds churn up "storm" conditions on the lake. (The chronic storminess of the lake was recorded in some passages of the New Testament.)

It is a well-known feature of fluid flow past rigid obstacles that regions of minimum pressure and maximum velocity form "above" some points of obstacle. For example, in the case of the laminar, creeping

[1] Now at Center for Earth and Planetary Physics, Harvard University, Cambridge, MA 02138.

0027-0644/82/080994-13$07.25

Stokes flow about a small rigid sphere, a region of maximum fluid velocity develops close to the sphere at about the intersection of the flow with a plane passing through the center of the sphere and perpendicular to the undisturbed flow. Such regions of maximum velocity appear also in turbulent flow, including atmospheric flow, around rigid obstacles. For some computational examples of flow about "mountains," see Mason and Sykes (1979, Figs. 3–6). The numerical calculations reported by Mason and Sykes tend to support the hypothesis that the strong winds of the Jordan Valley are primarily a result of frictionless fluid flow, but the conditions of (static) stability have a major influence on the time of development of the strong winds.

The purpose of this paper is to set forth a mesometeorological model to calculate the air flow from the Mediterranean past Lake Kinneret in summer. The earliest published research (known to us) on the form of the air circulation over the Jordan Valley in summer is a diagram prepared by the German meteorologist Ludwig Weickmann who visited Palestine during World War I. His diagram is republished in Ashbel (1951, Fig. 37). In Weickmann's chart the winds are westerly aloft which, we believe, is correct, but he also notes easterly winds near the ground on the west side of the Valley, a suggestion that is at variance with observations for the portion of the day from late in the morning until well after midnight.

The first numerical mesometeorological model aimed at understanding the features of the summer

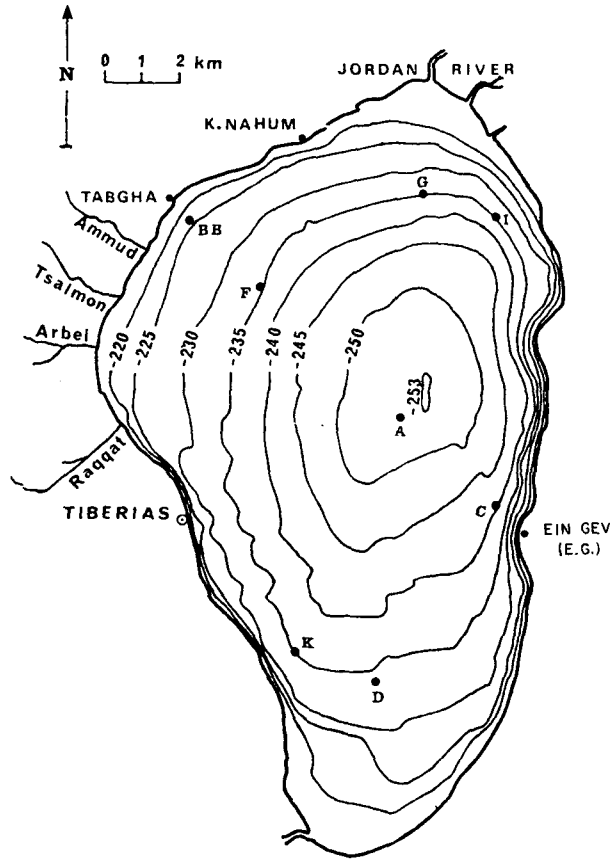

FIG. 2. Lake Kinneret. The western point is near Tabgha (BB) and the eastern is in Ein-Gev (E.G.). (Isopleths represent a bathymetric map; altitude in meters below MSL.)

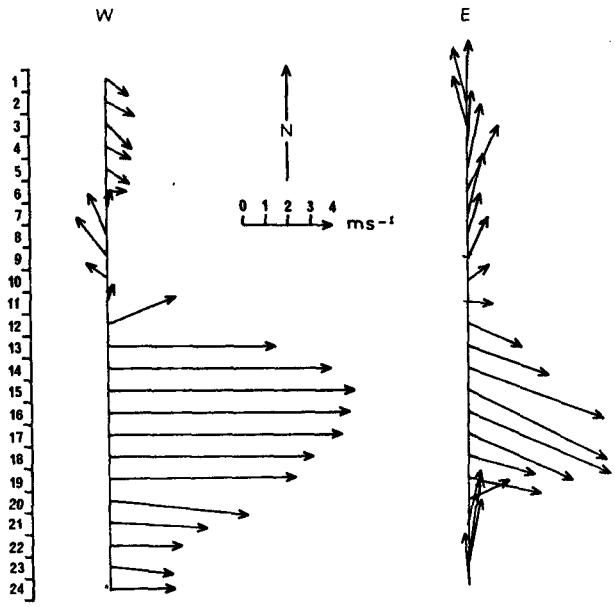

FIG. 1. The 24-hourly surface wind distribution at the western (Tabgha) and at the eastern (Ein-Gev) stations, after Serruya (1975).

circulation over the Lake Kinneret section of the Jordan Valley was developed by Doron and Neumann (1976). Their model, which is a forerunner of the model reported on in this paper, is, like the present one, a two-dimensional model with σ-coordinates. Their results predict fairly well some of the observed features of the circulation near the surface (e.g., the strong afternoon winds) in the Lake area, but some other features of their results were not satisfactory.

Anthes and Warner (1978b) prepared a mesometeorological model for the airflow over Israel, based on the σ-coordinate system. However, the lowest level of their model is at 290 m, making it impossible to compare their results with observations which are available only (at some points) near the surface. Another simulation of the flow over Israel is that of Mahrer and Segal (1979), which was not intended to simulate the summer flow; the simulated wind velocities in the Jordan Valley are not strong enough.

In preparing the present, improved model, we modified the formulation for friction and heating, increased the resolution of the model in the planetary boundary layer, improved the numerical methods

considerably and utilized the experience gained in earlier work with the σ-coordinate system.

2. Model

a. The equations

The model is two-dimensional, quasi-hydrostatic and assumes a steady large-scale geostrophic wind. With these assumptions, the equations of the model in the (x, σ, t) coordinate system are

$$\frac{\partial u}{\partial t} = -u\frac{\partial u}{\partial x} - \dot{\sigma}\frac{\partial u}{\partial \sigma} + f(v - v_g) - RT/(p_* + p_t/\sigma)\frac{\partial p_*}{\partial x} - \frac{\partial \phi}{\partial x} + F_x$$

$$\frac{\partial v}{\partial t} = -u\frac{\partial v}{\partial x} - \dot{\sigma}\frac{\partial v}{\partial \sigma} - f(u - u_g) + F_y$$

$$\frac{\partial \phi}{\partial (T/\theta)} = -c_p\theta$$

$$\frac{\partial \theta}{\partial t} = -u\frac{\partial \theta}{\partial x} - \dot{\sigma}\frac{\partial \theta}{\partial \sigma} + F_\theta$$

$$\frac{\partial p_*}{\partial t} = -\frac{\partial}{\partial x}(p_* u) - \frac{\partial}{\partial \sigma}(p_*\dot{\sigma})$$

$$\frac{\partial p_*}{\partial t} = -\int_0^1 \frac{\partial (p_* u)}{\partial x}\, d\sigma \qquad (1)$$

where

$$\sigma = (p - p_t)/(p_s - p_t) = (p - p_t)/p_*,$$

$$p_* = p_s - p_t,$$

and F_x, F_y, F_θ, are the expressions for the change of momentum and potential temperature due to vertical turbulent diffusion and are given by

$$\left.\begin{aligned} F_x &= \frac{g^2}{p_*^2}\frac{\partial}{\partial \sigma}\left(\rho^2 K_z \frac{\partial u}{\partial \sigma}\right) \\ F_y &= \frac{g^2}{p_*^2}\frac{\partial}{\partial \sigma}\left(\rho^2 K_z \frac{\partial v}{\partial \sigma}\right) \\ F_\theta &= \frac{g^2}{p_*^2}\frac{\partial}{\partial \sigma}\left(\rho^2 K_z \frac{\partial \theta}{\partial \sigma}\right) \end{aligned}\right\} \qquad (2)$$

The formulation for the vertical eddy viscosity K_z is introduced in the next section. Symbols are defined in the Appendix.

In the Israeli summer, phase changes of water are not important in the wind structure over Lake Kinneret. Thus we assume a "dry" model, and the humidity equation is neglected. For the horizontal diffusion we adopted a filter (see Section 3b).

b. Boundary conditions

The boundary condition at the lower and upper boundaries is $\dot{\sigma} = 0$ at $\sigma = 1$ and $\sigma = 0$. In addition, we assume $\partial u/\partial z = \partial v/\partial z = \partial \theta/\partial z = 0$ at $\sigma = 0$; i.e., there are no turbulent fluxes at the upper boundary. For the surface temperature we chose an expression similar to that used by Doron and Neumann (1976), i.e.,

$$T_s(\mathrm{K}) = 300 - 0.0065 z_G + E[11.79\sin(y + 0.376) + 5.73\sin(2y - 0.251) + 1.87\sin(3y - 1.1) + 0.69\sin(4y + 1.2)], \qquad (3)$$

where $y = 2\pi t/24$, t is time (hours) starting at 0800 LST, E is an amplitude function which increases linearly from 1 on the coast to 1.17 at a point 40 km inland (further inland this maximum amplitude is retained). Over the lake and sea we assume $E = 0.4$ and 0, respectively. Near the surface we assume $u = v = 0$ at $z = z_0$ (4 cm for land, 1 mm for water). The lateral boundaries are located far enough from the coast and from topographic gradients so that we may assume that the horizontal gradients of all fields vanish there, i.e.,

$$\frac{\partial u}{\partial x} = \frac{\partial v}{\partial x} = \frac{\partial \theta}{\partial x} = \frac{\partial p_*}{\partial x} = 0 \quad \text{at} \quad x = 0, L.$$

It was not necessary to add some special numerical treatment like "sponge" damping near the boundaries. The height of the level $\sigma = 1$ was fixed by the topography of a west–east cross-section of north Israel and thus

$$\phi(x, \sigma = 1, t) = g z_G(x). \qquad (4)$$

In the present experiments the top pressure of the model p_t was set equal to 750 mb. Further, in this version of the model there are no internal heat sources or sinks. We thus assume that the only heat exchange is with the lower boundary.

c. Initial conditions

The integrations are started at 0800 LST because, at that time, the surface temperatures (lake, sea and land) are close to the daily average. The initial temperature distribution is assumed to be divided into three layers, each with a constant lapse rate:

1) From the surface up to 930 mb, $\gamma = 0.0065$°C m^{-1}.
2) From 930–900 mb an inversion is assumed with $\gamma = -0.0015$°C m^{-1}.
3) From 900 mb to $p_t = 750$ mb, $\gamma = 0.0065$°C m^{-1}.

The inversion layer is assumed to represent the large-scale subsidence inversion present in summer

over the eastern Mediterranean coast. At $z = 0$, we put $p = 1000$ mb and $T = 300$ K. Next we calculate the initial surface pressure over the mountains by assuming a zero horizontal pressure gradient and making use of the above lapse rates. Without friction the initial winds are assumed to be geostrophic west-northwesterlies, with $\mathbf{V}_g = (u_g, v_g) = (3, -1)$ m s^{-1}. A few minutes after introducing the friction, an approximate Ekman geostrophic wind distribution is established with which we actually start the model experiment.

3. Turbulent transfer

a. *Vertical transfer*

According to (2), the vertical turbulent transfers are determined by the turbulent diffusivity K_z. It remains to specify K_z in terms of the mesoscale meteorological parameters predicted by the model. Several schemes were proposed in the literature based on various theories, but as yet there is no general agreement on a definite scheme suitable for both stable and unstable conditions.

For the initial experiments described in the present study, it was decided to use the formulation proposed by Blackadar (1978) in which K_z is given in the form

$$K_z = l^2 S f(\mathrm{Ri}),$$

where l is the mixing length, S the wind shear,

$$S = \left[\left(\frac{\partial u}{\partial z}\right)^2 + \left(\frac{\partial v}{\partial z}\right)^2\right]^{1/2},$$

and Ri the Richardson number,

$$\mathrm{Ri} = \frac{g}{\theta}\frac{\partial\theta/\partial z}{S^2}.$$

The mixing length is given by (Blackadar, 1962):

$$l = kz/(1 + kz/\lambda),$$

where k (the von Kármán constant) $= 0.4$ and $\lambda = 40$ m. The form chosen for the function $f(\mathrm{Ri})$ is:

$$f(\mathrm{Ri}) = (1 - 18\mathrm{Ri})^{1/2} \quad \text{for} \quad \mathrm{Ri} \leqslant 0$$

$$f(\mathrm{Ri}) = (1 + \alpha\mathrm{Ri})^2 \quad \text{for} \quad 0 \leqslant \mathrm{Ri} \leqslant -\alpha^{-1}$$

$$f(\mathrm{Ri}) = \begin{cases} 2 \text{ near the surface} \\ 1 \text{ elsewhere} \end{cases} \quad \text{for} \quad \mathrm{Ri} > -\alpha^{-1},$$

with $\alpha = -0.03$.

The formulation for the unstable case was recommended by Blackadar (1978) and the formulation for the stable case is according to Neumann and Mahrer (1971).

One of the problems with these two formulations is that they do not take into account surface roughness. It is natural to anticipate that in regions of steep topography, as in our case, the surface roughness z_0 is very large and thus we have increased drag near the surface. As this fact may have significant influence on the development of the flow patterns, it is desirable to include the effect at least in a crude fashion. For this purpose the following formulation for K_z is used for the lowest 10 m of the atmosphere. Specifically,

$$K_z = kz\bar{u}(C_D/2)^{1/2} = \frac{k^2 z\bar{u}}{\ln (z_1 + z_0)/z_0},$$

where C_D is the drag coefficient at $z_1 = 10$ m and $\bar{u}$ is the average wind speed for the layer. It should be said that, strictly speaking, the form of the equation applies to neutral conditions. In this way it is possible to prescribe z_0 in terms of the topography gradient and actual surface characteristics. As mentioned above, the present formulation is a tentative one for the purpose of the initial experiments. It is intended in the future to test several different formulations to assess their performance for the problem under discussion.

b. *Horizontal diffusion*

Instead of assuming a common formulation for horizontal diffusion, we adopted a highly selective low-pass filter proposed by Long *et al.* (1978) in the form

$$(1 - \delta)\bar{\Phi}_{j-1} + 2(1 + \delta)\bar{\Phi}_j + (1 - \delta)\bar{\Phi}_{j-1} = \Phi_{j-1} + 2\Phi_j + \Phi_{j+1},$$

where Φ is the field to be smoothed and $\bar{\Phi}$ the smoothed field. This implicit filter completely eliminates the $2\Delta x$ waves, while its smoothing effect on the longer wavelengths is a function of δ. The filter was successfully adopted by some authors (e.g., Mahrer and Pielke, 1978), who used it in models of sea-breeze and mountain flow.

4. Numerical aspects

This section presents a brief summary of the numerical formulation of the equations of the model.

A grid-point formulation was chosen for both the horizontal and the vertical directions. In the present version there are 65 points in the horizontal direction with a grid interval of 4 km. Ten levels were adopted for the vertical direction with a much better resolution near the ground than near the upper boundary: The first computational level is at 10 m and the height of any higher level is about twice the height of the level immediately below it, up to the top level (at 750 mb). Thus, the level altitudes above the surface are approximately: 10, 20, 35, 60, 110, 200, 350, 640, 1150 and 2100 m.

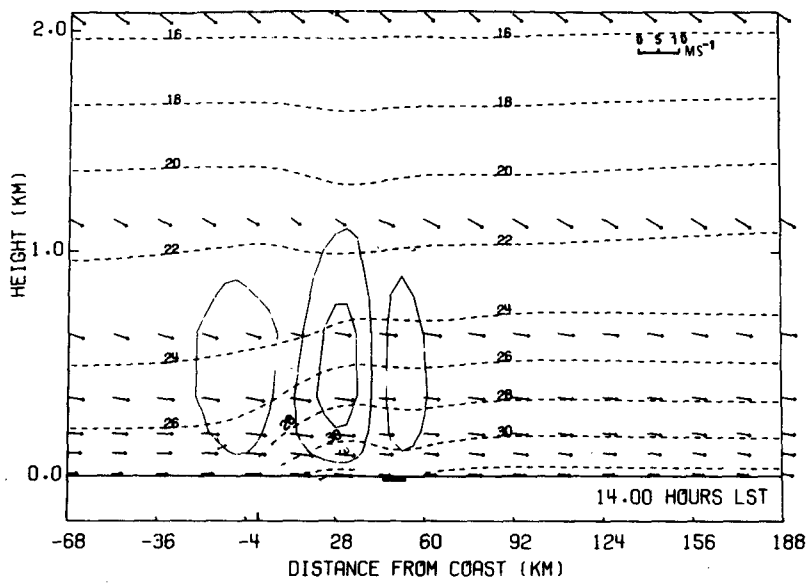

FIG. 3. Horizontal winds, m s^{-1} (arrows), vertical winds, cm s^{-1}, (solid lines) and temperatures, °C (dashed lines), at 1400 LST on the second day of calculation. Arrow bases are fixed at the level which they represent. Direction of arrows to right represents pure westerly wind, whereas the upward direction indicates southerly wind. Location of Lake Kinneret is illustrated by wider lower line. The horizontal wind scale is introduced in the upper right corner. Contour interval for vertical velocity is 2 cm s^{-1} (the closer inner curve is for 3 and the other of +1 and −1 cm s^{-1}).

To the horizontal terms of advection, pressure gradient and turbulent transfer, as well as to all other terms of the equations, we applied the split method of Marchuk (1974). Additionally, to avoid large truncation errors in regions of steep topography, the two terms representing the horizontal pressure gradient in the σ-coordinate system were combined into one term containing derivatives on a constant-pressure surface, following Kurihara (1968). This, of course, is combined with methods of interpolation from σ to pressure surfaces of the relevant variables, as suggested by Phillips in Morel (1973).

For the vertical diffusion terms, use is made of a semi-implicit scheme similar to the one proposed by Paegle *et al.* (1976) which we adapted to the σ-system.

For the horizontal advection terms, an upstream cubic spline interpolation is employed (e.g., Long and Pepper, 1976). This method avoids most of the problems of errors in phase speed and artificial diffusion encountered in conventional finite-difference interpolation.

As already mentioned (Section 3b), a numerical filter was used in the horizontal direction in place of explicit diffusion terms. This is an important contribution to the numerical handling of the equations. The advantages of this filter relative to the explicit filters are discussed by Alpert (1981).

5. Description of experiments and discussion

Several preliminary experiments, designed to test the various numerical schemes of the model, were performed. The preliminary experiments, which will not be described here, established the good performance of each of the components of the numerical schemes and increased our confidence in the validity of the results in the three principal experiments described in this section.

a. Experiment with level terrain, including friction and heating

In order to assess the influence of the special topographic features of the region, an initial reference experiment was performed with level terrain. Additionally, this experiment was used to compare the model's performance with several previous models for a level ground surface. In order to eliminate the influence of the initial conditions, the experiment was run for a period of 50–60 hours and the results presented are those of the second day. The horizontal and vertical wind distributions at 1400 LST are presented in Fig. 3.

In Fig. 3, a clear sea-breeze front may be seen some 30 km inland with vertical velocities up to 4 cm s^{-1}. Neumann and Mahrer (1971) published ear-

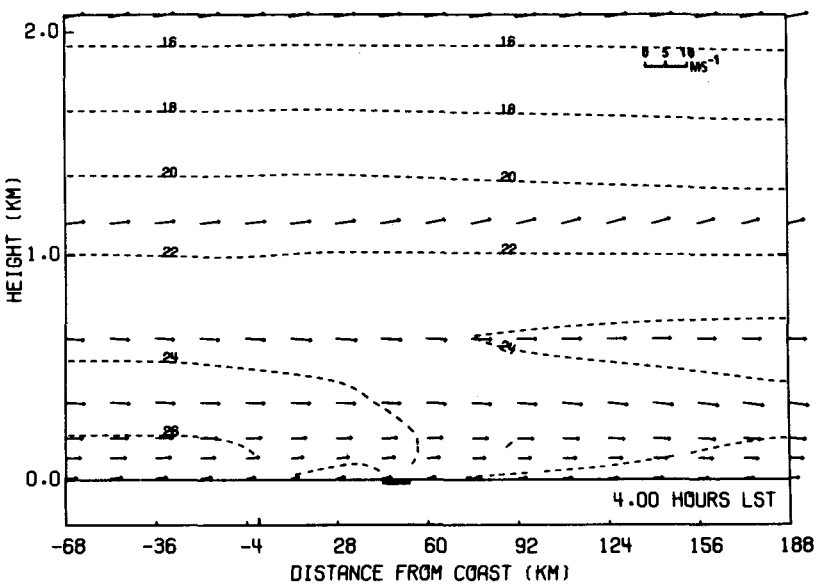

FIG. 4. As in Fig. 3 except at 0400 LST.

lier a mesometeorological model for a sea breeze over a level terrain but without a "lake" inland; moreover, in their model the large-scale pressure gradient was zero. In their results the sea-breeze front was located at 1400 LST about 40 km from the coast with maximum vertical velocities of $\sim$10 cm s^{-1}. The fact that, in the present experiment, the sea-breeze front did not penetrate farther is explained by the contrary effect of the Lake Kinneret breeze (the lake is located some 45 km from the Mediterranean coast). The existence of the lake breeze is evidenced by the downward motions observed over the lake, as opposed to the upward motion belt to the east and west of the lake. (The upward cell east of the lake is too weak to be observed, <1 cm s^{-1}.) The whole sea-breeze circulation is limited to the lower kilometer of the model, in part because of the inversion introduced at that level through the initial conditions. This inversion is, however, not maintained after the second day, because the mechanism responsible for it is a large-scale subsidence. This mechanism is not part of this mesoscale model and can only be introduced as an external forcing function. This was not done in the present initial experiments.

The model shows a maximum ground-level horizontal wind of $\sim$6 m s^{-1}, at $\sim$12 km from the coast, with an overall maximum of $\sim$8 m s^{-1} at this location, at a height of $\sim$110 m. This maximum intensifies to 9 m s^{-1} by 1600 LST and moves a few kilometers inland. By 1700 LST the sea-breeze front reaches the eastern shore of the lake, some 52 km from the Mediterranean coast. By that time, however, the whole circulation weakens appreciably.

The wind and temperature distributions at 0400 LST, just before sunrise, are shown in Fig. 4. This figure represents the maximum development of the land breeze. A well-established surface inversion is observed over the land, with temperatures in excess of 24°C at the top. In contrast to similar experiments (e.g., Neumann and Mahrer, 1971), no offshore easterly winds are observed and the only manifestation of the land breeze is a marked weakening of the westerlies near the coast. The reason for the discrepancy is the inclusion of a westerly geostrophic wind in the present model. In a similar experiment without a large-scale geostrophic wind, easterlies did develop near the sea coast. It appears that the presence of the large-scale (weak) westerlies is also responsible for the much weaker vertical winds ($\sim$0.4 cm s^{-1}), as compared to other experiments. The few available observations of vertical winds at the sea-breeze front also indicate stronger vertical winds than predicted by the model. Simpson *et al.* (1977) report vertical winds of up to 3 m s^{-1} at the sea-breeze front in southern England, where the width of the frontal region is only about 300–1000 m, suggesting the need for at least a similarly good model resolution. With a 4 km resolution, as in our model, the front is "smeared" and thus weaker vertical winds result. Repeating the experiment with a 2 km resolution did, in fact, give a much stronger front. This kind of resolution was, however, not practical for all of our experiments because of limitations on computer time. As the purpose of this initial work was to demonstrate the main effects of the topography on the sea- and lake-breeze circulations, the coarser resolution was maintained for all subsequent experiments.

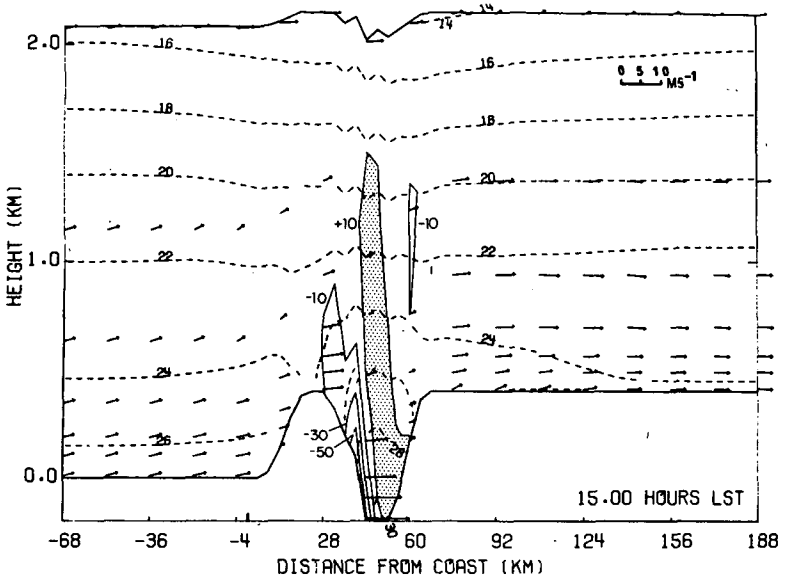

FIG. 5. As in Fig. 3 except at 1500 LST (first day) with topography, but without vertical friction and without heating. Contour interval for vertical wind is −20 cm s^{-1} (the extreme value above the western slope to the Lake is −50 cm s^{-1}). Upward motion areas (larger than 10 cm s^{-1}) are shaded.

b. Experiment with topography but without friction and heating

In the second experiment we added topography, but all other interactions with the lower boundary, i.e., all vertical subgrid-scale transport terms, were omitted. This experiment was designed to evaluate the adjustment of the flow field to the special geometry of the region. Since no forcing was involved, a more or less steady state was expected after a period of adjustment. It should, however, be pointed out that a true steady state is not possible in the model since a horizontal filter was included in the numerical work for computational stability. This acts as a sink for both kinetic and available potential energy, and thus the only possible steady state is a flow with no horizontal gradients in any fields. This sink is, however, small in intensity and a near-steady state does evolve after a period of about seven hours. It is interesting to note that a similar period of adjustment was also observed in an experiment with a diurnal cycle, i.e., the results of the first and second day of the run were very similar after this period.

The adjusted wind and temperature distributions are shown in Fig. 5. The main feature of the flow is the development of very strong downslope winds near the western edge of the Jordan Valley. This is consistent with similar results obtained in the lee of a single mountain ridge by several authors (Klemp and Lilly, 1978; Anthes and Warner, 1978a; Mahrer and Pielke, 1978). The maximum observed horizontal wind is ~15 m s^{-1} near the ground. In contrast, the upslope winds on the western side of the mountain (~10 km from the coast of the Mediterranean Sea) are very weak and only reach ~0.5 m s^{-1}. The same is true for the vertical velocities which reach a value of ~ −70 cm s^{-1} in the downward-motion cell and only 9 cm s^{-1} in the upward-motion cell.

The possible influence of reflected waves from the top to the interior was considered. According to experiments by Anthes and Warner (1978a), and Mahrer and Pielke (1978), it seems that whenever the diffusion over the entire domain is not too weak ($K_H \Delta t/\Delta x^2 \geq 10^{-2}$, as suggested by the former authors, K_H being the coefficient of horizontal eddy viscosity), then good simulation of mountain flow—at least in the lowest 1 km of the domain—is possible even without any absorbing layer near the top. In our simulation with $\Delta t = 8s$, $\Delta x = 4$ km, the above relation leads to a minimum value of $K_H \geq 2 \times 10^4$ $m^2 s^{-1}$. Instead of K-diffusion we used a selective low-pass filter ($\delta = 0.05$ in the equation in Section 3b) which introduced an even stronger diffusion for the shorter waves, with weaker diffusion to the longer wavelengths. Thus the effect of reflected vertical waves (induced by a relatively low mountain height of 0.4 km) is probably not important, at least in the lower 1 km.

A careful inspection of Fig. 5 reveals the existence of two-grid-point waves, especially in the temperature distribution in the vicinity of steep topography. Because the horizontal filter was not applied directly to the temperature field, but through the potential temperature, the existence of short-wave disturbances is to be expected.

On the basis of the results of the above two ex-

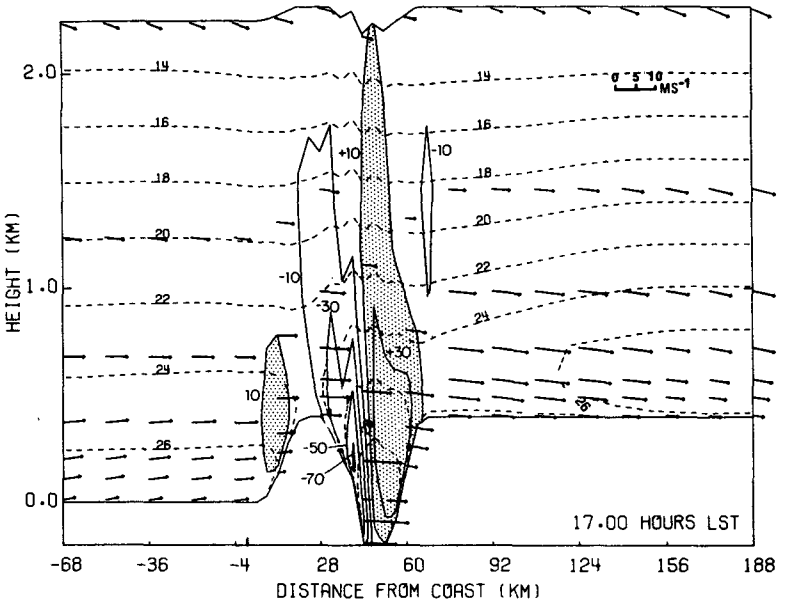

FIG. 6. As in Fig. 5 except at 1700 LST (first day) including heating and friction (extreme value for vertical wind above the western slope to Kinneret is −70 cm s^{-1}).

periments, it seems that both the model and the finite-difference formulations, as constructed, are capable of simulating the main dynamics of the mesoscale circulation reasonably well, even in the presence of topography.

c. *Experiment with topography and with friction and heating*

The third experiment of the series included the features of the first two experiments, i.e., a two-dimensional version of the full model, and was run for 48 hours. The flow patterns and temperature distributions at 1700 and 0400 LST are shown in Figs. 6 and 7, respectively. The principal features of the circulation at 1700 LST in the present experiment are similar to those obtained in Experiment B without vertical friction and heating. However, the vertical winds are somewhat stronger near the western shore of the lake than in the previous experiment. This seems to indicate that the main cause of the strong winds at the valley bottom in the afternoon hours is a dynamic effect due to geometrical forcing with only a secondary contribution by thermal effects.

The thermal effect plays a very important role in delaying the penetration of the downslope winds to the valley bottom. Whereas in the previous experiment strong winds appeared about four hours after the start of calculations, i.e., at about 1200 LST, they do not penetrate to the bottom until about 1500 LST in the present case. This is because of the upslope winds which develop on both sides of the valley, due to differential heating (anabatic winds). The existence of upslope winds is still evident on the western slopes of the hills near the Mediterranean coast where vertical winds of ~20 cm s^{-1} are observed in the present experiment, as compared with less than 10 cm s^{-1} in the previous one.

At 0400 LST, downslope (katabatic) winds are observed on both sides of the valley (Fig. 7). They are accompanied by a convergence zone and upward motion near the lake center. Due to the assumed westerly geostrophic wind, we observe stronger downslope winds on the western side than on the east. Near the sea coast, a classical land-breeze situation developed. In contrast to Experiment A (level ground), we actually observe southeasterly winds near the coast on land due to the combined effects of the land breeze and the katabatic winds. (For a more detailed analysis of the combined effects, see Doron and Neumann, 1977.) These easterly winds, in association with the offshore geostrophic westerlies, result in a convergence zone on the coast which probably is responsible for the early morning cloudiness observed in summer over the coastal region of Israel. It should be stressed that although the vertical winds near the coast are less than 10 cm s^{-1}, the combination of the convergence of humid air and relatively stable air aloft (say, 1 km), create favorable conditions for low stratus formation. This is, of course, not the case when stronger vertical motions develop *inland* by day, because the air is relatively dry.

The temperature profiles at four selected times and two selected points are presented in Figs. 8a and 8b.

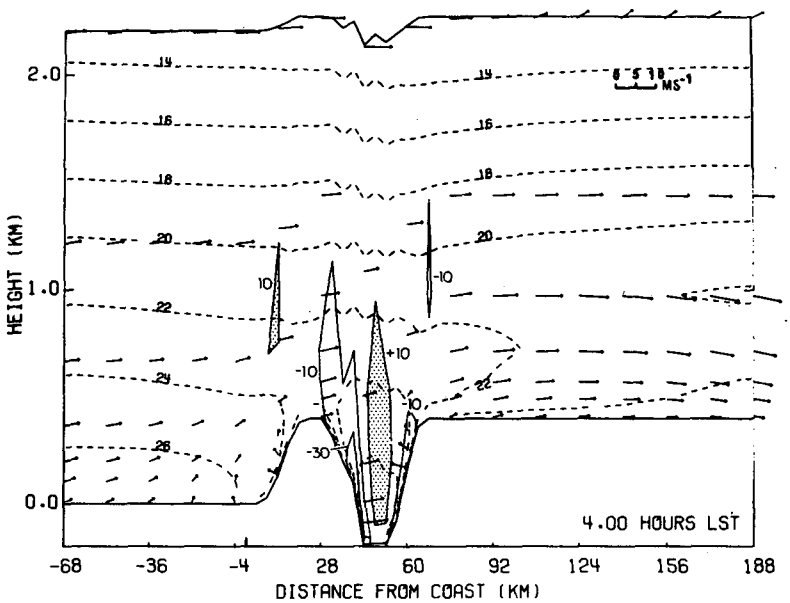

FIG. 7. As in Fig. 5 except at 0400 LST at the morning of third day.

The first point is 8 km from the coast at the foot of the hills and the second point is at the lake center. In Fig. 8a we observe the development of a nocturnal temperature inversion (at 2000 LST) which becomes stronger through the night; by morning (0600 LST), an isothermal layer up to ~200 m is prominent. During the day a strong super-adiabatic lapse rate (the average lapse rate from near the surface up to 10 m height is ~0.6°C m^{-1}, while between 10 and 20 m it reduces to ~0.06°C m^{-1}; above 200 m the lapse rate becomes stable) is observed above the ground (at 1400 LST), whereas above Lake Kinneret it is weaker and near the surface a shallow inversion layer (up to ~10 m) is predicted. Obviously, the

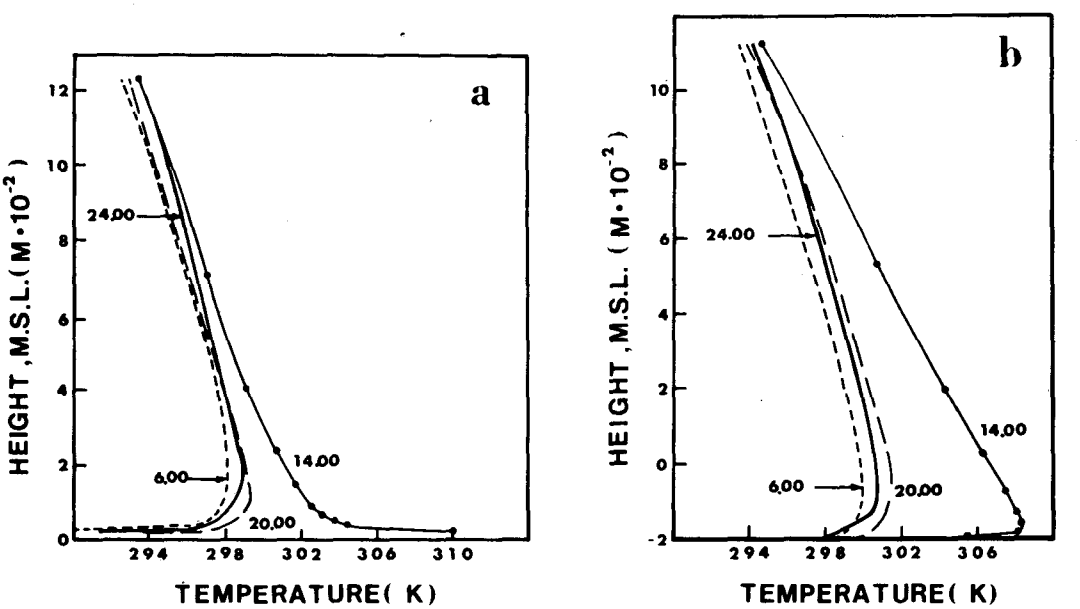

FIG. 8. Temperature profiles at four selected hours for (a) a point 8 km inland at 40 m height above MSL, (b) a point above the center of Lake Kinneret at −190 m MSL. The surface is approximately 10 m lower in both cases.

changes during the night are much weaker above the lake. In general, we may say that the vertical temperature profiles are very similar to those expected in the Israeli summer (excluding the subsidence inversion which cannot be maintained by the mesoscale processes).

The variation of the wind vector over the whole diurnal cycle at the lower level of the model on the western and eastern shores of the lake is shown in Fig. 9. For comparison, Fig. 9 also shows the observed winds, averaged for a two-week period in July (Serruya, 1975). On the western shore, the sudden penetration of the strong winds is evident both in the model and in the observations. With the observed winds, however, this happens shortly after midday, whereas in the model there is a delay of some two hours. Another discrepancy is that there is only a slight weakening of the wind toward nightfall in the model, whereas light winds are observed to prevail throughout the night. It seems that the effect of the mountain–valley winds is exaggerated by the model. Thus they delay the onset of downslope winds during the day and strengthen them at night. A similar exaggeration was noted by Anthes and Warner (1978b) in their simulation of parallel phenomena. There are some possible explanations to this exaggeration. Possibly, the particular points chosen on both shores are influenced greatly by the three-dimensional character of the topography involved. Even though the diurnal wind distribution at the eastern shore seems to be closer to the observed one, a closer look at the results shows that, in fact, the deviations on both

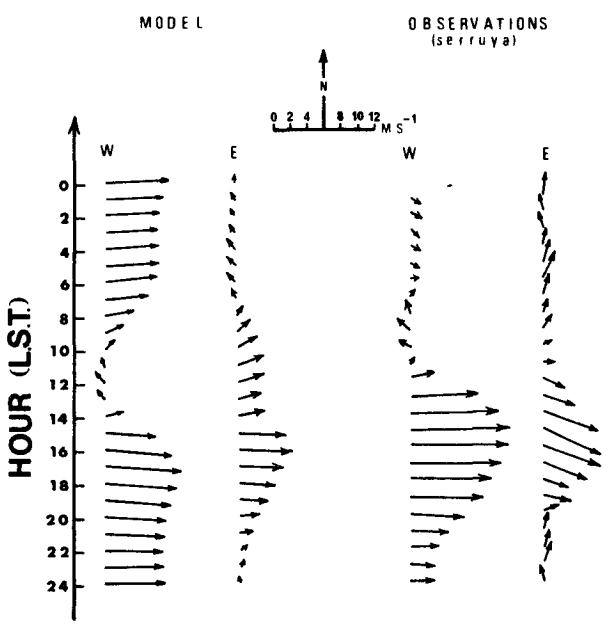

FIG. 9. 24-hourly surface wind distribution on the western and eastern shores of the lake—observed and calculated.

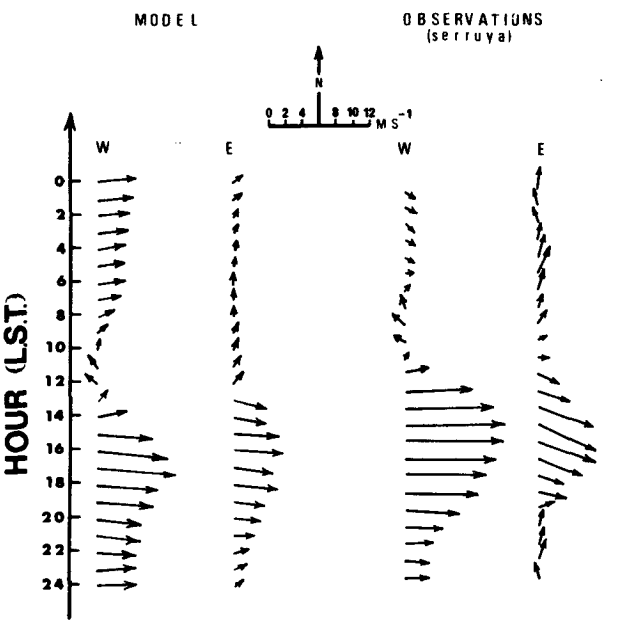

FIG. 10. As in Fig. 9, but after averaging (see text).

shores are in the same direction. The convergence over the lake in the afternoon is simulated very well considering our two-dimensional model. Unfortunately, no upper air observations are available in the region, so no check could be made on the circulation at elevated points.

In Fig. 10, as in Fig. 9, we again illustrate both the predicted wind model and the observed winds; however, the model results have now been averaged. The averaging was done in the following manner: in the afternoon the values at shore points were averaged with neighboring points inland while the rest of the time they were averaged with neighboring points above the lake. The purpose of this averaging form is to overcome the effect of smoothing that is introduced by the horizontal filter. This smoothing is particularly vigorous in an area of large gradients and, to partially remove its effect (clearly not by reducing the diffusion to a point where the model becomes numerically unstable), we suggest an averaging with a neighboring point only from one side. For example, in the afternoon, only the west neighbor (on shore) was chosen since the anticipated stronger wind was smoothed by the relatively weaker winds above the lake. Following this reasoned procedure of averaging, we get results that better fit the observations. In particular, notice how the observed weakening of the wind on the western coast is better predicted in Fig. 10.

Fig. 11 illustrates the difference between the surface pressure and the average surface pressure in the model domain at two points, one some 8 km inland from the coast and the other over the lake center.

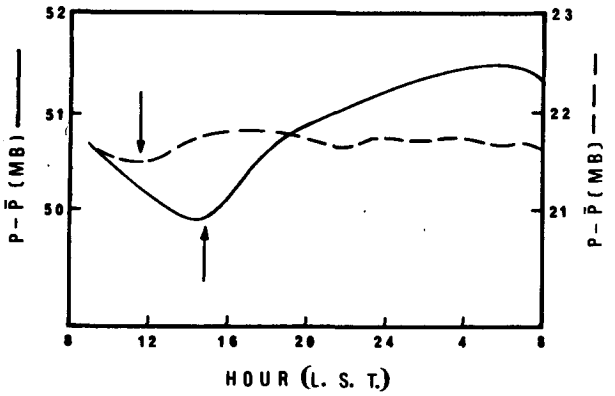

FIG. 11. Differences between surface pressure and average surface pressure in the domain for two points; one (dashed line, right scale) 8 km inland from the coast and the other (solid line, left scale) over the lake center. Arrows show times of breeze arrival.

The difference, rather than the pressure itself, was chosen because the average surface pressure in the model is not quite conserved, due to the open boundary conditions. In the experiment without topography, this caused a change of about 0.5 mb per day in the average surface pressure, but the change amounts to a few mb per day in the experiment with topography. The reason for this is that the thickness of the atmosphere is very different on the two lateral boundaries, so the mass flux is also very different.

The pressure drop on land due to the sea-breeze circulation is apparent in Fig. 11, with an amplitude of some 0.2 mb near the coast and about 1 mb on the lake. The high amplitude of the diurnal pressure wave in the Jordan Valley is a well-known fact (Ashbel, 1951). The observations, however, indicate a significantly larger amplitude than the one predicted by the model. The sudden penetration of the westerly winds into the valley is accompanied by a sudden rise in surface pressure—a typical occurrence on the passage of the sea-breeze front.

Now we would like to discuss further the reasons for the intensity of the winds regularly observed at the west shore of the lake. Obviously, the development of strong lee winds in inviscid fluids behind an obstacle is very important. This was, in fact, visualized through Experiment B. However, thermal effects are vital for this unique phenomenon in two different ways. First, the contribution of the lake breeze to the upslope winds gives relatively strong easterlies on the western slope of the Kinneret Valley. These winds, caused by differential heating, prevent the westerly MSB from penetrating into the valley. Thus, the "outbreak" of the cool Mediterranean air becomes possible only with the weakening of the easterlies as the differential heating passes its peak.

Secondly, the relatively cool Mediterranean air contributes to the acceleration of the air at the lee slope of the mountains; this is a density current. In fact, when calculating the values of the air densities we found that between 1300 and 1500 LST the density above the mountain top increases, while at the same altitude above the lake the density decreases. Obviously, this is caused by two mechanisms: thermal heating in the valley, and continued advection of cool Mediterranean air at the mountain top. Eventually, this leads to a change in sign of the horizontal density gradient at ~1500 LST. This contribution cannot be neglected, because the dynamic effect (as shown in Experiment B) cannot account for the intensities observed when friction is included. Also, there is nothing unusual in strong surface lee winds for an inviscid fluid: they have been reported by many investigators (see, e.g., Mahrer and Pielke, 1978).

6. Summary and conclusions

The results of the experiments described in the previous section represent a reasonable simulation of the important circulation features both near the Mediterranean coast and in the Lake Kinneret Valley.

It appears that the effects of the topography in northern Israel on the development of the diurnal wind variation and structure, can be understood through the use of a two-dimensional model. It must be noted, however, that in the present version of the model, surface temperatures are prescribed and the model is based on a crude representation of the diabatic heating processes in the atmosphere. A realistic heat-balance equation near the surface, along with a more sophisticated representation of both the turbulent and radiative heat-transfer processes in the atmosphere, are essential for future experiments with the model. Whereas no marked deviations from measured fields are observed in the region between the western hills and the coast, there are some discrepancies in the Kinneret Valley. These include about a two-hour delay in the penetration of the westerly winds to the lake, and the persistence of the relatively strong winds on the western shore until morning. The fact that, despite the expected katabatic winds at night and the westerly geostrophic winds, the eastern shore of the lake remains almost calm, as observed, remains unexplained. One possible reason is that the actual momentum transfer to the surface is quite large due to the relatively warm lake. Returning to our problems in simulating the western shore calculation, it should be mentioned that the whole subject of momentum and heat transfer near the ground, in regions of steep and rugged topography, is poorly understood. There is a need for more satisfactory formulations, combining the results of both theoretical investigations and field experiments.

An important question which is often asked, concerns the ability of quasi-hydrostatic models to simulate mesoscale flows in the presence of steep topography. On the basis of the experiments described here, it appears that there is still much to learn with the help of such models and that the discrepancies observed do not seem to be connected with non-hydrostatic effects.

Another point which needs investigation is the influence of changing horizontal resolution in the model. There seems to be no doubt that the present resolution of 4 km will not be sufficient for more refined experiments. For example, the frontal region of the sea breeze definitely needs a much better resolution. It is probable that a significantly smaller grid distance would give a much more enhanced circulation.

The results reported here should thus be regarded as an encouraging first step toward the development of a realistic mesoscale model and through it a better understanding of the processes governing the circulation.

Acknowledgments. The authors wish to thank Y. Mahrer for his helpful suggestions, and especially for the advanced plot programming. We want to thank A. Huss for the useful discussions. Special thanks to D. Cohen for the design of the program and to other advisors at the Computing Center, Hebrew University of Jerusalem.

This work has been summarized while one of the authors (Alpert) was a visiting Research Fellow in Dynamical Meteorology at the Center for Earth and Planetary Physics, Harvard University. Dr. Alpert was supported while at Harvard by National Science Foundation Grant ATM 78-23330. We wish to thank R. S. Lindzen for his helpful remarks.

APPENDIX

List of Symbols

C_D	drag coefficient
c_p	specific heat at constant pressure
F_x, F_y, F_θ	changes of west–east momentum, south–north momentum and potential temperature due to turbulent diffusion, respectively
f	Coriolis parameter
g	acceleration of gravity
k	von Kármán's constant
K_H	horizontal eddy viscosity
K_z	vertical eddy viscosity
l	mixing length
L	lateral extent of model
p	pressure
p_*	$\equiv p_s - p_t$
p_s, p_t	pressure at surface, and top of the model atmosphere, respectively
R	gas constant for air
Ri	Richardson number
S	wind shear
T	temperature
t	time
u, v	west–east and south–north velocities, respectively
u_g, v_g	as in the entries for u, v but for the geostrophic wind
$\mathbf{V}$, $\mathbf{V}_g$	vectors for horizontal wind and horizontal geostrophic wind, respectively
x, y	west–east, south–north coordinates
y	$\equiv 2\pi t/24$ [Eq. (3) only]
z	vertical coordinate
z_0	roughness parameter
z_1	≈ 10 m
z_G	ground elevation
α	$\equiv -0.03$, nondimensional constant in diffusion formulation
γ	lapse rate
δ	smoothing parameter for the filter
Δt	= 8 s, time increment
Δx	= 4 km, space increment in x direction
λ	= 40 m, parameter in diffusion formulation
ρ	density
σ	$= (p - p_t)/p_*$
$\dot{\sigma}$	vertical σ-velocity [$\equiv d\sigma/dt$]
ϕ	geopotential height
Φ_j, $\bar{\Phi}_j$	field values before and after smoothing
θ	potential temperature.

REFERENCES

Alpert, P., 1981: Implicit filtering in conjunction with explicit filtering. *J. Comput. Phys.*, **44**, 212–219.

Anthes, R. A., and T. T. Warner, 1978a: Development of hydrodynamic models suitable for air pollution and other mesometeorological studies. *Mon. Wea. Rev.*, **106**, 1045–1078.

——, and ——, 1978b: Simulation of mesoscale flows over Israel. *Israel Meteor. Res. Pap.*, **2**, 93–123.

Ashbel, D., 1951: *Regional Climatology of Israel.* Dept. Atmos. Sci., Hebrew University of Jerusalem, 244 pp.

Blackadar, A. K., 1962: The vertical distribution of wind and turbulent exchange in a neutral atmosphere. *J. Geophys. Res.*, **67**, 3095–3102.

——, 1978: *High Resolution Models of the Planetary Boundary Layer. Advances in Environmental and Scientific Engineering*, Vol. 1. Gordon and Breach, 276 pp.

Doron, E., and J. Neumann, 1976: Difficulties and results of a mesometeorological model with topography. Presented at Conf. Army Mesometeorological Research, Las Cruces, NM, Dept. Atmos. Sci., Hebrew University of Jerusalem, 29 pp.

——, and ——, 1977: Land and mountain breezes with special attention to Israel's Mediterranean coastal plain. *Israel Meteor. Res. Pap.*, **1**, 109–122.

Klemp, J. B., and D. K. Lilly, 1978: Nonlinear numerical simulation of hydrostatic mountain waves. *J. Atmos. Sci.*, **35**, 78–107.

Kurihara, Y., 1968: Note on finite different expressions for hy-

drostatic relation and pressure gradient force. *Mon. Wea. Rev.*, **96,** 654–656.

Long, P. E., W. A. Shaffer, J. E. Kemper and F. J. Hicks, 1978: The state of the Techniques Development Laboratory's boundary layer model May 24, 1977. NOAA Tech. Memo. NWS TDL 66, Silver Spring, MD, 63 pp.

——, and D. W. Pepper, 1976: A comparison of six numerical schemes for calculating the advection of atmospheric pollution. *Preprints, Third Symp. on Atmospheric Turbulence, Diffusion and Air Quality*, Raleigh Amer. Meteor. Soc., 181–187.

Mahrer, Y., and R. A. Pielke, 1978: A test of an upstream spline interpolation technique for the advective terms in a numerical mesoscale model. *Mon. Wea. Rev.*, **106,** 818–830.

——, and M. Segal, 1979: A numerical study of the air flow over Israel using a two-dimensional mesoscale model. *Preprints, Fourth Conf. on Numerical Weather Prediction*, Silver Spring, Amer. Meteor. Soc., 256–259.

Marchuk, G. I., 1974: *Numerical Methods in Weather Prediction.* Academic Press, 277 pp.

Mason, P. J., and R. I. Sykes, 1979: Separation effects in Ekman layer flow over ridges. *Quart. J. Roy. Meteor. Soc.*, **105,** 129–146.

Morel, P., Ed., 1973: *Dynamic Meteorology.* D. Reidel, 622 pp.

Neumann, J., and Y. Mahrer, 1971: A theoretical study of the land and sea breeze circulation. *J. Atmos. Sci.*, **28,** 532–542.

Paegle, J., W. J. Zdunkowsky and R. M. Walch, 1976: Implicit differencing of predictive equations of the boundary layer. *Mon. Wea. Rev.*, **104,** 1321–1324.

Serruya, S., 1975: Wind, water temperature and motions in Lake Kinneret: General pattern. *Verh. Int. Verein. Limnol.*, **19,** 73–87.

Simpson, J. E., D. A. Mansfield and J. R. Milford, 1977: Inland penetration of sea-breeze fronts. *Quart. J. Roy. Meteor. Soc.*, **103,** 47–76.